SCIENCE CHINA
Physics, Mechanics & Astronomy

• Article •

March 2021 Vol. 64 No. 3: 034711
https://doi.org/10.1007/s11433-020-1652-x

Analytic derivation of Monin-Obukhov similarity function for open atmospheric surface layer

Yong Ji, and Zhen-Su She*

State Key Laboratory for Turbulence and Complex Systems and Department of Mechanics and Engineering Science, College of Engineering, Peking University, Beijing 100871, China

Received September 29, 2020; accepted December 22, 2020; published online January 25, 2021

The Monin-Obukhov (MO) similarity function ϕ_m of the atmospheric surface layer (ASL) describing the deviation from the log law of the canonical turbulent boundary layer because of thermal stratification has been traditionally determined empirically. This study presents a unified analytic expression derived from a symmetry-based theory of wall turbulence, called structural ensemble dynamics (SED), which postulates a generalized dilation symmetry principle expressing the effect of the wall on turbulence, leading to an analytic multi-regimes expression for the mixing length. For ASL in unstable and stable conditions (i.e., UC and SC), a unified two-regime formula of the mixing length is proposed, leading to a ϕ_m, similar to the Businger-Dyer (BD) formula; with a simplified model energy balance equation, ϕ_m is completely specified with no free parameter. Furthermore, the theory allows the study of the open ASL's underlying additional physical processes such as bottom-up or top-down flux due to pressure variations T_p. Assuming that T_p is decomposed into shear-like and buoyancy-like components, we propose new explanations for two important features of typical ASL: a significantly smaller Karman constant of 0.36 and a varying ϕ_m for SC mean speed profiles. The theory is validated by the data obtained at Kansas and also at Qingtu Lake Observation Array in Northern China for a variety of heat flux conditions. In conclusion, due to pressure variations, we assert that ASL is intrinsically open and that the current theory offers a new basis for its quantification.

Monin-Obukhov similarity theory, open atmospheric surface layer, boundary layer turbulence, symmetry-based analysis

PACS number(s): 47.55.Hd, 47.20.Ky, 92.60.Fm

Citation: Y. Ji, and Z.-S. She, Analytic derivation of Monin-Obukhov similarity function for open atmospheric surface layer, Sci. China-Phys. Mech. Astron. **64**, 034711 (2021), https://doi.org/10.1007/s11433-020-1652-x

1 Introduction

The atmospheric surface layer (ASL) is the hinge region where the earth surface exchanges mass and energy with the atmosphere through turbulence. The understanding and quantification of turbulent processes in ASL are important not only for the fundamental study of the boundary layer with high Reynolds number (Re) [1], but also for the applications [2] of numerical weather prediction and modeling of pollution diffusion and sand storm. In general, the two most important processes in ASL are earth surface-induced "wall" shear and thermal stratification due to air temperature variation; the latter is recognized as the main cause for the deviation of the wind speed profile from the famous log law. However, ASL is an intrinsically open system involving the interaction with the upper atmosphere, where large-scale motions due to pressure variation are frequent. This study aims to develop a theory that allows the study of the effect of thermal stratification and bottom-up and top-down effects due to pressure fluctuations.

Earlier, Monin and Obukhov (MO) [3,4] proposed a simi-

*Corresponding author (email: she@pku.edu.cn)

larity theory with variable $\zeta \equiv z/L$, where L, now called Obukhov length, is defined as $L = -u_\tau^3/\left(\kappa \langle w'T' \rangle g/\bar{T}\right)$, where u_τ is the friction velocity, κ is the Karman constant, w' and T' is the vertical speed and temperature fluctuations, respectively, and $\langle w'T' \rangle$, $\bar{T}$, and g refers to the heat flux, mean temperature profile, and gravitational acceleration respectively. In the MO theory [3], the most remarkable quantity is the nondimensional similarity function:

$$\phi_m(\zeta) = \frac{\kappa z}{u_\tau} \frac{\mathrm{d}U}{\mathrm{d}z}, \tag{1}$$

where U is the mean speed profile. Once ϕ_m is known, one can readily predict U by an integration. It is known that $\phi_m(\zeta)$ cannot be derived from dimensional analysis alone, and thus, more theoretical arguments need to be introduced. First, one assumes that $\phi_m(0) = 1$ as the heat flux approaches zero, or $L \to \infty$ (thus, $\zeta \to 0$), and the log law is recovered, corresponding to the neutral ASL. This assumption will be proved to be incorrect by the present study, which shows that a non-negligible pressure-induced flux yields a finite deviation of ASL from a canonical TBL, manifesting in a much smaller Karman constant of 0.36 [5].

Furthermore, the effect of thermal stratification on ϕ_m has been traditionally determined by fitting the experimental data through a measured wind speed U. One of the most popular formulas is presented by Businger et al. [6] and Dyer [7], hereafter referred to as BD formula, which takes the following form: $\phi_m(\zeta) = (1 - 15\zeta)^{-1/4}$ when $\zeta < 0$ (for UC) with upward heat flux during daytime, and $\phi_m(\zeta) = 1 + 4.7\zeta$ when $\zeta > 0$ (for SC) with downward heat flux during nighttime. The BD formula had been confirmed by many observations, including well-known Kansas experiments. Moreover, Carl et al. [8] suggested another formula with a slightly different scaling exponent ($-1/3$) to better fit some UC data: $\phi_m(\zeta) = (1 - 15\zeta)^{-1/3}$. It seems that the data do not support a single formula, so a better understanding of the variability of the observed $\phi_m(\zeta)$ is required. An implicit form of ϕ_m has been proposed based on a simplified turbulent kinetic energy balance equation, yielding the so-called O'KEYPS (after Obukhov, Kazansky, Ellison, Yamamoto, Panofsky, and Sellers) equation [9]: $(\phi_m(\zeta))^4 - \gamma\zeta\,(\phi_m(\zeta))^3 = 1$, where γ is an empirical constant ranging from 5 to 18 in different reports. The variability of γ is an intriguing issue, for which this study will develop an alternative point of view that it is a direct consequence of the pressure variations (see sect. 3.4).

More recently, Katul et al. [10] pursued a path to relate the turbulent energy spectrum to the mean velocity [11], yielding also an equation to determine $\phi_m(\zeta)$ as:

$$\phi_m(\zeta)^4 - \zeta\phi_m(\zeta)^3 = \frac{1}{f(\zeta)}, \tag{2}$$

where $f(\zeta)$ is a dimensionless function describing the effect of thermal stratification in terms of eddy's anisotropy. It is able to yield a different power law of $\phi_m(\zeta)$ for a different heat flux regime, whose prediction agrees reasonably well with some UC data. However, for SC, its prediction has a substantial deviation, which is later corrected by Salesky et al. [12] using a stability-dependent integral lengthscale. Instead, Li et al. [13] introduced a new length, called the Ozmidov scale L_{OZ}, to form a new similarity variable $\zeta' = z/L_{\mathrm{OZ}}$, replacing ζ to construct $f(\zeta)$. In summary, these spectrum-based models explain some aspects of the scaling of ϕ_m and parameters, but need the knowledge about integral length to predict ϕ_m. Since the model spectrum only involves inertial subrange, it is thus conceptually difficult to consider nonequilibrium effect of very large-scale motions. Indeed, it is already known that to describe SC or analyze turbulent intensities [14], the model needs to introduce more lengths and spectral relations, thus depending on too many fitting parameters. Viewing the current state-of-the-art, a new approach is needed to achieve a concise yet comprehensive description of ASL.

This paper presents explicit forms of $\phi_m(\zeta)$ for both UC and SC in a unified way, based on a newly developed theory of wall turbulence, called structural ensemble dynamics (SED) [15-18], which develops a renovative Lie-group symmetry analysis on the momentum and energy balance equations. The SED theory defines several stress lengths that extended from the classical mixing length and introduces a generalized dilation symmetry assumption. In each flow region, the lengths behave in a power law in z (height), owing to the invariant energy balance mechanism in the region where the dilation symmetry of lengths in z is preserved. Furthermore, across different regions, a universal symmetry breaking is postulated, yielding a specific transition function connecting different power laws. Proceeding from the wall to the entire flow domain, the theory then yields a multiregime expression and the predicted (entire) mean velocity and turbulence kinetic energy profiles are validated with unprecedented accuracy by several dozens of experimental and numerical profiles in a wide range of *Re* of canonical wall turbulence [15-18]. It is intriguing to see whether the theory applies to ASL to yield a unified description that is also adaptive to a variety of physical situations related to the complexity of the atmospheric turbulence.

Below, a unified two-regime formula of Reynolds stress length ℓ_{13} for both UC and SC is presented, leading to a similar expression as the BD formula. A remarkable feature of the present theory is that it allows further analysis for open ASL underlying different physical processes such as bottom-up or top-down flux due to pressure variations T_p. Specifically, a reasonable argument can be developed to determine the transition parameters (from shear-dominated to heat flux-

dominated regime), ζ_{UC} (or γ in BD), and ζ_{SC} (or β in BD) by solving a simplified vertical turbulent kinetic energy balance equation with an isotropic dissipation. An outstanding feature of this analysis is that it can be extended to include the effect of pressure variations and thus establish a quantitative framework to study the open ASL underlying bottom-up or top-down flux due to pressure variations T_p. The theory is fully validated by the well-known Kansas data and the data measured at Qingtu Lake Observation Array (QLOA) in Northern China for a variety of heat flux conditions, which allows for a preliminary determination of pressure effect and for an explanation of two important features of typical ASL: a significantly smaller Karman constant of 0.36 and varying ϕ_m for SC mean speed profiles. In summary, a unified analytic expression of ϕ_m has been derived for the first time, in both UC and SC with bottom-up and top-down energy fluxes. This study asserted that ASL is intrinsically open due to pressure variations and that the present theory has achieved a definitive step for a comprehensive description of real (nonequilibrium) ASL.

2 Data

An important aspect of the present work is to validate the theory by observational data. In addition to the famous Kansas data, we have specifically analyzed data at QLOA, which is built on the dry lake bed located in Minqin County, Gansu Province, in Northwestern region of China. In spring, sustained northwest monsoon flows through the observation site of which the surface relief is less than 1 m within 10 km in the upwind direction. It is an ideal field laboratory for observation of ASL since it presents a high *Re* turbulent boundary layer which could reach a friction *Re* of the order of 10^6, much larger than laboratory wind tunnel experiments. The array which consists of 21 towers, one main tower of 32 m high and 20 other lower towers of 5 m high, are organized into a T-like shape. The wind speeds are measured by a sonic anemometer with a 50-Hz sampling frequency, and observations have been carried out day and night throughout several years, offering abundant data for all weather conditions. Several studies on large-scale motion, energy spectrum, etc., at clear time or during sand storm have yielded interesting results on the physics of ASL, see refs. [19-21].

Here, wind speed measurements are analyzed in the main tower, equipped with 11 anemometers of approximate logarithmic equidistance from 0.9 to 30 m. 12 sets of data are selected for UC during May 23, 2014, and 11-h samples of data are chosen for SC during the nights of May 23 and March 27, 2014, since long-duration data with large enough wind speed are more rare in nighttime. The detailed information of the data is shown in Table 1. The friction velocities are selected to be larger than 0.2 m/s and the Obukhov length ranges from −96.4 to 351.0 m, covering unstably, neutrally, and stably stratified ASL. The corresponding similarity coordinate ranges from −4.9 to 1.1, which is wide enough to validate the present SED similarity theory.

Table 1 The information of QLOA data used in this paper

No.	Time and date	u_τ (m/s)	L (m)
1	2014-05-23 7:00-8:00	0.28	−96.4
2	2014-05-23 8:00-9:00	0.31	−22.8
3	2014-05-23 9:00-10:00	0.32	−13.5
4	2014-05-23 10:00-11:00	0.33	−11.4
5	2014-05-23 11:00-12:00	0.34	−11.4
6	2014-05-23 12:00-13:00	0.29	−7.7
7	2014-05-23 13:00-14:00	0.33	−10.4
8	2014-05-23 14:00-15:00	0.29	−6.1
9	2014-05-23 15:00-16:00	0.30	−9.8
10	2014-05-23 16:00-17:00	0.34	−16.9
11	2014-05-23 17:00-18:00	0.39	−27.2
12	2014-05-23 18:00-19:00	0.35	−36.8
13	2014-03-27 0:00-1:00	0.26	31.0
14	2014-03-27 1:00-2:00	0.59	237.6
15	2014-03-27 2:00-3:00	0.67	351.0
16	2014-03-27 3:00-4:00	0.59	350.5
17	2014-03-27 4:00-5:00	0.48	263.9
18	2014-03-27 5:00-6:00	0.41	259.4
19	2014-03-27 6:00-7:00	0.31	134.9
20	2014-03-27 7:00-8:00	0.25	143.8
21	2014-05-23 2:00-3:00	0.22	27.5
22	2014-05-23 6:00-7:00	0.21	47.2
23	2014-05-23 20:00-21:00	0.23	40.6

3 Theory

3.1 Energy balance analysis

We begin by analyzing turbulent kinetic energy (TKE) equation to identify different energy balance regimes. Instead of treating the full TKE equation, we choose to discuss each component of TKE equation separately, following Kader and Yaglom [22], since the heat flux effect important to ASL acts only in the vertical component. Indeed, ref. [22] claimed that $\kappa^4 L$ is the real vertical scale in ASL.

In what follows, we assume that the ASL flow is statistically stationary and the averaged quantities only depend on z, independent of x (streamwise direction). Therefore, the TKE equations are [22]

$$\langle u'w'\rangle \frac{\mathrm{d}U}{\mathrm{d}z} + \rho^{-1}\left\langle p'\frac{\partial u'}{\partial x}\right\rangle = \varepsilon_u + \frac{1}{2}\frac{\partial\left\langle u'^2 w'\right\rangle}{\partial z}, \tag{3}$$

$$\rho^{-1}\left\langle p'\frac{\partial v'}{\partial y}\right\rangle = \varepsilon_v + \frac{1}{2}\frac{\partial\left\langle v'^2 w'\right\rangle}{\partial z}, \tag{4}$$

$$\langle w'T'\rangle\frac{g}{\bar{T}} + \rho^{-1}\left\langle p'\frac{\partial w'}{\partial z}\right\rangle + \rho^{-1}\frac{\partial\langle p'w'\rangle}{\partial z} = \varepsilon_w + \frac{1}{2}\frac{\partial\left\langle w'^3\right\rangle}{\partial z}. \tag{5}$$

Eqs. (3)-(5) corresponds to the streamwise, spanwise, and vertical energy balance equation, respectively, where x, y, z are the streamwise, spanwise, and vertical coordinates, v' is the spanwise velocity fluctuation, p' is the pressure fluctuation, $\varepsilon_u, \varepsilon_v$ and ε_w are the dissipation of the three directions.

In ASL, turbulence production mechanisms mainly include shear production for streamwise component and buoyancy production for the vertical component. For convenience, we use $S = \langle u'w'\rangle\frac{\mathrm{d}U}{\mathrm{d}z}$ to denote the shear production which converts the mean motion energy to a streamwise fluctuation, and $B = \langle w'T'\rangle\frac{g}{\bar{T}}$ to denote buoyancy production, which injects heat energy to the vertical fluctuation. The terms involving p on the left hand side are denoted by R_u, R_v and R_w. The second terms of the right-hand side are denoted by T_u, T_v and T_w and the pressure transport is denoted by T_p. The equation could then be rewritten as:

$$S + R_u = \varepsilon_u + T_u, \tag{6}$$

$$R_v = \varepsilon_v + T_v, \tag{7}$$

$$B + R_w + T_p = \varepsilon_w + T_w. \tag{8}$$

In our following discussion, higher-order turbulent transport terms are ignored, but the effect of T_p in sect. 3.4 will be considered below. Note that in canonical TBL, T_p is absent. Our present study reveals primary importance in ASL, representing transport by large-scale pressure variation. Hunt et al. [23,24] argued its importance in ASL even in near-neutral conditions.

The pressure-strain correlation term redistributes energy in three directions, leading the turbulence to a small-scale isotropic state. Following Bou-Zeid et al. [25] who neglected turbulent transport, the energy equation is simplified by assuming a small-scale isotropy for dissipation:

$$\varepsilon_u = \varepsilon_w = \varepsilon_v = \varepsilon/3. \tag{9}$$

Furthermore, the sum of turbulent production, dissipation, and buoyancy is zero (i.e., $S + B = \varepsilon$), and the sum of three pressure redistributions terms is also zero (i.e., $R_u + R_v + R_w = 0$). Thus, eqs. (6)-(8) could be rewritten as:

$$R_u = -\frac{2}{3}S + \frac{1}{3}B, \tag{10}$$

$$R_v = \frac{1}{3}S + \frac{1}{3}B, \tag{11}$$

$$R_w = -\frac{2}{3}B + \frac{1}{3}S. \tag{12}$$

This indicates that pressure redistribution terms (R_u, R_v and R_w) can be expressed in terms of shear (S) and buoyancy (B), owing to the energy balance equation. Normalizing eqs. (6)-(8) by S, all R terms become an explicit function of the Richardson number $Ri_f = -B/S$. This was validated by a simulation data [25]. Note that the Richardson number is generally a function of the height. Below, we will show that it reaches specific values for shear-dominated and buoyancy-dominated regimes, so that the critical Ri_f may be derived to specify the transition point between the two regimes. Below, all different regimes in ASL will be enumerated and an analysis of the Richardson number is presented.

Typical regimes of ASL can be described in the following energy balance scenario:

- Neutral: turbulent energy mainly originates from shear production and balanced by the dissipation, $S = \varepsilon$, two-third of which are redistributed from streamwise to vertical and spanwise components: $R_u = -2\varepsilon/3$ and $R_w = R_v = \varepsilon/3$.
- SC: turbulent energy is generated by the shear production mainly balanced by the buoyancy. Because turbulence must be sustained, there exists a minimum dissipation $\varepsilon_\mathrm{m} \ll S$. R_u redistributes $S - \varepsilon_\mathrm{m}/3$ to vertical and spanwise components, $R_v = \varepsilon_\mathrm{m}/3$ and $R_w = S - 2\varepsilon_\mathrm{m}/3$, respectively. So, in the vertical direction, $S - \varepsilon_\mathrm{m}$ balances B.
- Strongly SC: dissipation is negligible, so shear production S is balanced by R_u: $R_u = -S$ is almost entirely redistributed to the vertical component, $R_w \approx -R_u = S$, while the spanwise component is negligible: $R_v \approx 0$.
- UC: buoyancy balances the dissipation in the vertical direction, $B = \varepsilon/3$. Shear production generates two-thirds of the dissipation: $2\varepsilon/3$, half of which is redistributed from streamwise to the spanwise component: $R_u = -\varepsilon/3$ and $R_v = \varepsilon/3$.
- Strongly UC: in the extreme case of UC, buoyancy provides turbulent energy in all three directions, $B = \varepsilon$, two-thirds of which, $2\varepsilon/3$, are equally redistributed to streamwise and spanwise directions. i.e., $R_u = R_v = \varepsilon/3$.

The above results are summarized in Table 2. Note that the neutral, UC, and strongly UC regimes could be similar to dynamic, dynamic-convective, and convective regimes, respectively, as first suggested by Kader and Yaglom et al. [22,26] who, however, have not clearly defined the transition parameters. A more detailed study of the correspondence will be reported elsewhere.

A key outcome of the above analysis is to derive a critical Richardson number marking the transition between UC (or SC) and the neutral situation. We postulate the following reasonable criteria: the transition point is located where the two sinks (i.e., buoyancy B and dissipation ε) are equal for SC, or where the two sources (buoyancy B and pressure redistribution R_w) are equal for UC. The rational behind these criteria

Table 2 The energy balance in different regimes as special solutions to eqs. (10)-(12). Note that the two transition regimes are determined by the relations: $B+S=\varepsilon$ and $-B/S=Ri_f$

Case	S	B	R_u	R_v	R_w	Ri_f
Strongly SC	$-B$	$-S$	$-S$	≈ 0	S	~ 1
Transition 1	$4\varepsilon/3$	$-\varepsilon/3$	$-\varepsilon$	$\varepsilon/3$	$2\varepsilon/3$	$1/4$
Neutral	ε	0	$-2\varepsilon/3$	$\varepsilon/3$	$\varepsilon/3$	0
Transition 2	$5\varepsilon/6$	$\varepsilon/6$	$-\varepsilon/2$	$\varepsilon/3$	$\varepsilon/6$	$-1/5$
Strongly UC	≈ 0	ε	$\varepsilon/3$	$\varepsilon/3$	$-2\varepsilon/3$	$-\inf$

is clear: the middle of the transition corresponds to the situation where buoyancy grows and gradually reaches the same magnitude as the prevalent sink or source. With these criteria, one can readily derive the critical Richardson number: for SC, $Ri_f = 1/4$, since $R_w/B = -2$ (see eq. (12)); or for UC, $-Ri_f = 1/5$, since $R_w/B = 1$ and $R_w + B = \varepsilon/3$. Note that the latter result is also consistent with ref. [27], which showed that the transition point marks the beginning of the decreasing momentum transport efficiency. The two critical transition Richardson numbers are also presented in Table 2, which will be used below to determine the two critical transition parameters.

3.2 Extended SED analysis

The SED is a similarity theory of wall turbulence [15,16] that is based on the following basic assumptions:

(1) In the thin boundary layer, the Reynolds averaged Navier-Stokes (RANS) equation has its solution strongly constrained by the dilatation-group invariance in the direction normal to the wall. This symmetry constraint manifests in a series of stress lengths, defined by the Reynolds stresses and the mean shear, physically describing the dominant eddy sizes relevant to turbulent diffusivity. The relevant stress length for vertical momentum diffusion is the Prandtl mixing length: $\ell_{13} = \sqrt{W_{13}}/\partial_z U$, where $W_{13} = -\langle u'w'\rangle$.

(2) The boundary layer is composed of several subregions and within each subregion, turbulent motions are self-organized into a similarity state so that $\ell_{13} \sim z^{\alpha}$ (also called the structural ensemble). It is assumed that the subregion (or structural ensemble) is formed due to a single dominated mechanism of energy balance. In other words, the transition from one subregion to another is due to the change of the underlying energy balancing mechanism.

(3) It is assumed that across two subregions, a dilation symmetry-breaking occurs with a variation of scaling exponent $\alpha \to \alpha'$, and the transition function is universal.

For instance, in the region where turbulence production $W_{13}\partial_z U$ balances dissipation ε, $\ell_{13} \approx \kappa z$ (linear scaling in z) and the famous log law follows. Closer to the wall, it is shown [15,16] that there exists a viscous sublayer where energy dissipation balances diffusion and $\ell_{13} \propto z^{3/2}$, while further away from the wall, a buffer layer occurs where the streamwise turbulent fluctuation reaches the maximum and the turbulent transport then balances the residue dissipation (e.g., the subtraction of dissipation and diffusion) and $\ell_{13} \propto z^2$. More remarkably, because the universal transition takes place from layer to layer, a unified expression called multi-layer formalism is derived and validated, describing all structural ensembles of varying energy balancing mechanism. This is a typical feature of wall shearing turbulence involving nonequilibrium dynamics (e.g., transport in space and across scales). Note that ℓ_{13} is interpreted to quantify the size of eddy that contributes to the momentum transport in the vertical direction in the SED theory.

The SED theory takes a fundamentally different approach to the closure problem of turbulence. Instead of solving a specific set of balance equations by a closure model, we consider the symmetry constraint on all balance equations and postulate a global feature valid for all Reynolds stresses, namely the formation of several structural ensembles, originating from different energy balance mechanisms. Ref. [16] shows that knowing ℓ_{13}, one can solve the closed mean momentum equation and obtain the mean velocity profile (MVP). Ref. [17] further shows ℓ_{11}. ℓ_{22} and ℓ_{33} display similar multi-layer structure as ℓ_{13} (up to a few small anomalies). The distribution of three turbulence intensities could then be described analytically. The predicted intensity distributions are validated with an unprecedented accuracy for the canonical channel, pipe, and turbulent boundary layer against a large variety of numerical and experimental data. Thus, according to the SED theory, the dominant physics in wall turbulence is the dilation symmetry-breaking associated with the change of the energy balance mechanism. While a general concept (i.e., dilation symmetry-breaking) is still pending further elucidation, its validated mean velocity and kinetic energy profiles are strong evidence of its consistency with all budget equations.

Now, we follow the SED theory to derive the formula of ℓ_{13} for ASL , in which dominant energy balance mechanisms are already known. The two dominant energy regimes in ASL are the shear dominant regime at low height where the wall's

effect is strong, and the heat flux dominant regime where TKE mainly originates from buoyancy production. In the shear dominant regime near the bottom of ASL, $\ell_{13} \approx \kappa z$, following the linear law of the mixing length theory by Prandlt. As the height increases, shear production $S \sim 1/\ell_{13}$, which decreases as z^{-1} while the heat flux is constant in ASL. Thus, there exists a critical transition point above which buoyancy production begins to play a role. There are two situations where the heat flux dominates: upward and downward heat flux, corresponding to UC and SC, respectively.

For UC with complete control by the heat flux, $\phi_m(\zeta) \sim (-\zeta)^{-1/3}$, following dimensional analysis [8] or an expansion argument [28]. Then, eq. (1) yields: $\partial_z U \sim u_\tau(\kappa z)^{-1}(-\zeta)^{-1/3}$. Since $\sqrt{W_{13}} \approx u_\tau$, we obtain: $\ell_{13} \sim \kappa z(-\zeta)^{1/3}$. Then, a two-regime formula of the SED theory yields (see Appendix A1)

$$\ell_{13}^{\wedge} = \kappa\zeta\left(1 - \frac{\zeta}{\zeta_{\rm UC}}\right)^{1/3}, \qquad \zeta < 0, \tag{13}$$

where $\kappa = 0.45$ is Karman constant [16], $\zeta_{\rm UC}$ is the critical transition parameter, similar to γ in BD and Carl's formula.

For SC, buoyancy absorbs TKE and dissipation, resulting in different scaling compared to the UC. Considering an extreme situation that the energy produced by the shear is almost completely absorbed by buoyancy, then $W_{13}\partial_z U \sim -B$. Eq. (1) then yields: $\ell_{13} \sim W_{13}^{3/2}/(-B)$. Since $W_{13} = u_\tau^2$, we could obtain $\ell_{13} \sim u_\tau^3/(-B)$ which is proportional to the Obukhov length. In other words, in strong SC, the size of eddies in charge of momentum transport approaches to a constant, which is proportional to the Obukhov length L. In this case, the two-regime formula of ℓ_{13} as derivation in Appendix A2 reads,

$$\ell_{13}^{\wedge} = \kappa\zeta\left(1 + \frac{\zeta}{\zeta_{\rm SC}}\right)^{-1}, \qquad \zeta > 0, \tag{14}$$

where $\zeta_{\rm SC}$ is the critical transition parameter, above which $\ell_{13}^{\wedge}$ deviates from the linear law, similar to β in the BD formula. While γ and β in the BD formula are determined by fitting empirical data, the present symmetry-based theory is able to derive them (i.e., $\zeta_{\rm UC}$ and $\zeta_{\rm SC}$) based on its definition as the transition height of the energy balancing mechanism, as shown below in sect. 3.3.

Now, we are ready to write down the full expression for ϕ_m. According to the definition:

$$\phi_m = \frac{\sqrt{W_{13}}}{\ell_{13}} \times \frac{\kappa z}{u_\tau}, \tag{15}$$

we are able to obtain

$$\phi_m \approx \begin{cases} \left(1 - \dfrac{\zeta}{\zeta_{\rm UC}}\right)^{-1/3}, & \zeta < 0, \\ 1 + \dfrac{\zeta}{\zeta_{\rm SC}}, & \zeta > 0. \end{cases} \tag{16}$$

3.3 Analytic derivation of critical transition parameter $\zeta_{\rm UC}$ and $\zeta_{\rm SC}$

We now present an argument to derive the critical transition parameters, $\zeta_{\rm UC}$ and $\zeta_{\rm SC}$, contained in the expressions of the stress length (eqs. (13) and (14), respectively). The basic assumption behind this derivation is the simplified model energy balance equation neglecting pressure effect and turbulent transport, described in sect. 3.1. Under this assumption, the only relevant terms specifying vertical variations are the shear production S and the buoyancy heat flux B that combine to a single parameter, which is the Richardson number $Ri_f = -B/S$. In ASL, at both UC and SC, the energy balancing mechanism varies from the shear-dominated regime at a lower height to the buoyancy-dominated regime at an upper height. Thus, the magnitude of Richardson number increases monotonically in z and the critical Richardson number will define the critical height for both UC and SC (i.e., $\zeta_{\rm UC}$ or $\zeta_{\rm SC}$).

First, note that Ri_f can be related to ℓ_{13}: $Ri_f = -B/S = -BW_{13}^{-1/2}\ell_{13} = -Bu_\tau^{-1}\ell_{13}$. A rescaling with Obukhov length yields

$$Ri_f = \begin{cases} \zeta\left(1 - \dfrac{\zeta}{\zeta_{\rm UC}}\right)^{1/3}, & \zeta < 0, \\ \zeta\left(1 + \dfrac{\zeta}{\zeta_{\rm SC}}\right)^{-1}, & \zeta > 0. \end{cases} \tag{17}$$

At the transition point, i.e., $\zeta = -\zeta_{\rm UC}$ (for $\zeta < 0$) or $\zeta = \zeta_{\rm SC}$ (for $\zeta > 0$), takes the critical Richardson number argument (its values presented in Table 2): $Ri_f = -1/5$ or $Ri_f = 1/4$, and we find

$$\begin{aligned} \zeta_{\rm UC} &= 0.2/2^{1/3} \approx 0.16 = 1/6.3, \\ \zeta_{\rm SC} &= 0.25/2^{-1} \approx 0.5 = 1/2. \end{aligned} \tag{18}$$

This yields

$$\phi_m \approx \begin{cases} (1 - 6.3\zeta)^{-1/3}, & \zeta < 0, \\ 1 + 2\zeta, & \zeta > 0. \end{cases} \tag{19}$$

Comparing eq. (19) with the BD formula, one can readily derive an equivalent value of BD's parameter: $\gamma \approx 1/\zeta_{\rm UC} \approx 6.3$ and $\beta \approx 1/\zeta_{\rm SC} \approx 2$. This theoretical determination is achieved entirely based on an analysis of the energy balance equation for the first time. Note that the predicted γ and β seem to be noticeably smaller than the empirical values ($\gamma \approx 16$ and $\beta \approx 4.6$) from fitting a large variety of data. This deficiency inspires a further investigation by considering more physics of ASL such as additional pressure-induced vertical energy transport.

3.4 Pressure effect: possible pressure transport

As mentioned earlier, ASL turbulence is an open system affected constantly by a large-scale inhomogeneity because of pressure fluctuations, whose contribution to vertical energy balance is expressed by T_p term and neglected in our derivation above. This term may be related to the so-called top-down effect, as earlier speculated by Hunt et al. [23, 24] and supported by previous analysis of QLOA observations [19]. Note that Salesky et al. [12] argued that the spatial transport, including pressure transport, is not important in ASL. We believe this is false for small to large heat flux regime. The imbalance was also recently noticed by Chamecki et al. [29], who put forward a TKE-based framework for studying the disturbed ASL and found that the vertical fluctuation intensity is affected. We now demonstrate that the SED theory offers a basis for the systematic treatment in the energy balance equation of additional terms (source or sink) since the symmetry-based approach is still valid to deal with the constraints imposed by a wall (i.e., earth surface for ASL).

Below, we outline briefly a preliminary consideration, but leaves a thorough investigation of the pressure transport in a future communication. This consideration adds the following assumption to that stated in sect. 3.2: the pressure transport has a vertical structure (i.e., z-dependence) which, at least in leading order, can be decomposed into the two most important energy modes, namely shear production S and buoyancy heat flux B. Specifically, we assume that

$$T_p = aS + bB, \tag{20}$$

where a and b are two free parameters used to quantify the pressure-induced vertical energy transport. The rationale behind this assumption is that at very large Reynolds number, the turbulent boundary layer has essentially two kinds of components: active and inactive, as proposed earlier by Townsend [30]. The former forms attached eddies whose size is proportional to the wall distance, like S, while the latter corresponds to some large-scale action which introduces a constant energy flux, like B in ASL. We conjecture that these two components originate from wall symmetry constraints that are preserved even when vertical pressure transport is not negligible. Then, the new energy balance equations can be written in a similar form to eqs. (6)-(8)

$$S' + R'_u = \varepsilon_u, \tag{21}$$

$$R_v = \varepsilon_v, \tag{22}$$

$$B' + R'_w = \varepsilon_w, \tag{23}$$

where $S' = (1+a)S$, $B' = (1+b)B$, $R'_u = R_u - aS$, $R'_w = R_w + aS$. Consequently, the transition point is defined by $B'/S' = -1/5$ for UC, $B'/S' = 1/4$ for SC.

Now, three different situations are considered to elucidate the effect of active (aS) and inactive (bB) components:

- UC under the effect of active component: $a \neq 0, b = 0$.

For UC at the transition point, the ratio of B' and S' satisfies

$$\left.\frac{B'}{S'}\right|_{\zeta=-\zeta_{\rm UC}} = \left.\frac{B}{(1+a)\frac{\partial U}{\partial z}W_{13}}\right|_{\zeta=-\zeta_{\rm UC}} = -\frac{1}{5}. \tag{24}$$

The active part of T_p contributes to the momentum transport in ASL, so ℓ_{13} will be modified. However, this modification only changes the slope or the Karman constant κ by a factor of $1 + a$. It can be verified whether

$$\ell^{\wedge}_{13} = (1+a)0.45\zeta\left(1 - \frac{\zeta}{\zeta_{\rm UC}}\right)^{1/3}, \quad \zeta_{\rm UC} \approx 0.16. \tag{25}$$

Eq. (24) is satisfied $\left(\text{taking } W_{13} \approx u_\tau^2,\ L = -\frac{u_\tau^3}{\kappa B}\right)$. The above result shows that the active component of T_p modifies the Karman constants but does not shift the transition height.

- SC under the effect of active component: $a \neq 0, b = 0$.

Similar result is obtained for SC and the resulting stress length is

$$\ell^{\wedge}_{13} = (1+a)0.45\zeta\left(1 + \frac{\zeta}{\zeta_{\rm SC}}\right)^{-1}, \quad \zeta_{\rm SC} = 0.5. \tag{26}$$

- UC under the effect of inactive component: $a = 0$, $b \neq 0$.

For UC at the transition point, the ratio of B' and S' satisfies

$$\left.\frac{B'}{S'}\right|_{\zeta=-\zeta_{\rm UC}} = \left.\frac{(1+b)B}{\frac{\partial U}{\partial z}W_{13}}\right|_{\zeta=-\zeta_{\rm UC}} = -\frac{1}{5}. \tag{27}$$

In this case, $\ell^{\wedge}_{13}$ is not modified but a shift of $\zeta_{\rm UC}$ takes place by a modification of B:

$$\ell^{\wedge}_{13} = 0.45\zeta\left(1 - \frac{\zeta}{\zeta_{\rm UC}}\right)^{1/3}, \quad \zeta_{\rm UC} = \frac{0.16}{1+b^-}. \tag{28}$$

- SC under the effect of inactive component: $a = 0, b \neq 0$.

For SC, the same derivation yields

$$\ell^{\wedge}_{13} = 0.45\zeta\left(1 + \frac{\zeta}{\zeta_{\rm SC}}\right)^{-1}, \quad \zeta_{\rm SC} = \frac{0.5}{1+b^+}. \tag{29}$$

- The general situation: $a \neq 0, b \neq 0$.

The above results show that the active component aS only affects the slope of $\ell^{\wedge}_{13}$, while the inactive component only affects the transition height $\zeta_{\rm UC}$ and $\zeta_{\rm SC}$. Since the energy balance equation is linear in T_p, the general situation is a superposition of the two effects. Thus, we obtain

$$\ell^{\wedge}_{13} = \begin{cases} (1+a)\zeta\,(1 - 6.3(1+b^-)\zeta)^{1/3}, & \zeta < 0, \\ (1+a)\zeta\,(1 + 2(1+b^+)\zeta)^{-1}, & \zeta > 0. \end{cases} \tag{30}$$

The results presented below compared to data indicate that $a \approx -0.2$ for both Kansas and QLOA data, while b seems to be different for different sites. More discussions are presented in sect. 4.

The corresponding similarity function ϕ_m is

$$\phi_m \approx \begin{cases} (1+a)^{-1}\,(1-6.3(1+b^-)\zeta)^{-1/3}, & \zeta < 0, \\ (1+a)^{-1}(1+2(1+b^+)\zeta), & \zeta > 0. \end{cases} \tag{31}$$

Finally, the analysis is completed by presenting a formalism for the prediction of U, which is made only for the increment beyond the lowest measured speed, $\Delta U_i = U_i - U_1$, to avoid complexity with consideration of roughness effect (which will be discussed elsewhere). According to the definition of the stress length, the MVP could be predicted by an integration:

$$\Delta U(i) = \int_{h_1}^{h_i} \frac{u_\tau}{\ell_{13}} \mathrm{d}z, \tag{32}$$

where h_i is the height of ith measurement probe. With the model described in eq. (20), our prediction formula can be explicitly written as:

$$\Delta U_i = \frac{u_\tau L}{1+a} \int_{h_1}^{h_i} \mathrm{d}z/z \begin{cases} (1-6.3(1+b^-)z/L)^{-1/3}, & L < 0, \\ (1+2(1+b^+)z/L), & L > 0. \end{cases} \tag{33}$$

4 Validation

Now, the present theory is validated with data. It is important to directly validate eq. (13) (or eq. (14)), which requires to derive ℓ_{13} from mean speed measurement of QLOA. To accurately calculate $\mathrm{d}U/\mathrm{d}z$ (and hence ϕ_m) from the mean speed data U, we follow ref. [31] using log-polynomial to fit the mean speed data:

$$U = c_0 + c_1 \log(z) + c_2 \log(z)^2. \tag{34}$$

The main tower of QLOA contains 11 observation points in the vertical direction that offers adequate points to fit. Each time, we pick five adjacent points along z to determine the coefficients c_0, c_1. and c_2. The gradient is then calculated as $\mathrm{d}U/\mathrm{d}z = c_1/z + 2c_2 \log(z)/z$.

The measured ℓ_{13} is compared with the theoretical prediction, as shown in Figure 1 for UC and SC. Symbols are the values derived from mean speed measurements at QLOA (black) and Kansas (red). It can be seen that when $|\zeta|$ is less than 0.1, $\ell_{13}^\wedge$ satisfies the linear law. As $|\zeta|$ increases, $\ell_{13}^\wedge$ shows different trends in UC and SC. For UC, the scaling exponent of ℓ_{13} changes to 4/3 as predicted by the analysis, indicating that the buoyancy stretches the size of the attached eddy in charge of the momentum transport. The dashed (blue) line is the SED prediction without any fitting parameter (i.e., no effect of pressure transport, $T_p^\wedge = 0$). For UC, as shown in Figure 1(a), this impressively agrees well with the measurements even in heat flux-dominated regime at $-\zeta > 0.1$ but slightly deviates from data in the near-neutral condition ($|\zeta| \sim 0.1$). This (slight) deviation is corrected by the introduction of $a = -0.2$.

For SC, Figure 1(b) shows a more interesting result. ℓ_{13} is globally shifted down from the canonical log law for small ζ, corresponding to a smaller Karman constant close to 0.36 (with $a \approx -0.2$) compared to either classical value (0.4) or new SED value (0.45). According to the present work, this is an indication of pressure transport: $T_p \approx -0.2S$. The same correction takes place in UC but the resulting change in ℓ_{13} is less remarkable in Figure 1(a). Here, a single $a \approx -0.2$ is chosen for both UC and SC to fit the data and thus, the continuity at $\zeta = 0$ is guaranteed. This then yields a typical Karman constant of 0.36, which is consistent with a previous study [5]. The minus sign of a implies taking away of

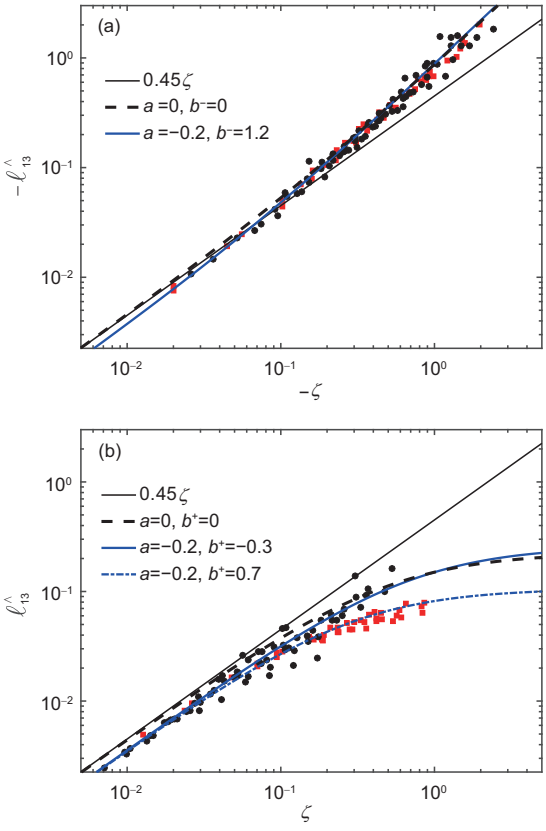

Figure 1 (Color online) Normalized stress length by Obukhov length $\ell_{13}^\wedge = \ell_{13}/L$ versus ζ for UC (a) and SC (b). Black symbols are the derived data from the mean speed measurement at QLOA, and the red squares are those that are calculated from the Kansas data using eq. (1). The lines correspond to the theoretical predictions. Solid black lines are the log law for canonical TBL; dash black lines are the predictions of the current theory with no pressure effect: $T_p = 0$ (eq. (13) for UC and eq. (14) for SC with parameter given by eq. (18)). Blue lines correspond to a simple model for pressure effect: $T_p = aS + bB$. Note that at small $|\zeta|$, the deviation from canonical law is much more remarkable for SC (b) than for UC (a).

turbulent energy by T_p, which is consistent with the picture that the active shearing turbulent structure is generated in the bottom and transported upward. This is also called the bottom-up process.

On the other hand, Figure 1(b) reveals a nonzero and different b for Kansas and QLOA data: $b \approx 0.7$ for Kansas data (dotted blue line) and $b \approx -0.3$ for QLOA data (solid blue line). A positive b for SC indicates an enhancement of the downward energy flux induced by pressure transport (at night) at Kansas site, while an opposite (upward) flux is introduced at QLOA site. Is this related to the fact that the Kansas's surface condition is wheat farming, while QLOA has a flat dry lake bed surface? More study should be carried out later. Note that the Kansas data extends in ζ much further away in SC (up to $\zeta \approx 1$) in clear distinction from QLOA data. Clearly, the parameter b is not universal but depends on the surface condition. Thus, it is intriguing to study the near-surface T_p effect using the parameter b, which can be obtained by fitting measured mean speed data, as will be done below.

Next, we discuss ϕ_m, which is presented in Figure 2, displaying the comparison between several theoretical predictions and data, for which both Kansas (red squares) and QLOA (black circles) data are included. Note that the Karman constant is traditionally involved in the calculation of ϕ_m from the mean speed measurement data. Kansas data originally assumes $\kappa = 0.4$. So when ϕ_m is extracted from literature, we need to multiply a factor of $0.45/0.4$ since we assume $\kappa = 0.45$ here. The green line is from the BD equation, while the black dashed line is from the Katul's spectral model (with at least three fitting parameters). The blue line is predicted by the present SED theory (with the model $T_p = aS + bB$). A far view from Figure 2 seems to indicate that all models are in reasonable agreement with data, but a closer view at small $|\zeta|$ from the inset of Figure 2 indicates that the SED agreement is better than the BD and Katul's results.

The inset of Figure 2 reveals a remarkable finding that both UC and SC do not pass through $\phi_m(0) = 1$. In other words, we assert (based on the SED assumption $\kappa = 0.45$) that the near-neutral ASL (of small heat flux) at both Kansas and QLOA sites are distinctly different from canonical (or wind tunnel) wall turbulence (of zero heat flux). Moreover, there is a significant contribution from pressure transport that yields a smaller Karman constant. This conclusion holds for both unstable and stable situation. For UC, it is much more visible from ϕ_m plot than from ℓ_{13} plot (Figure 1(a)); instead of $\phi_m(0) = 1$, actually $\phi_m(0) \approx 1.26$, indicating a bottom-up flux for both cases. This explanation for smaller Karman constant raises an issue for debate, and more data should be studied in the future.

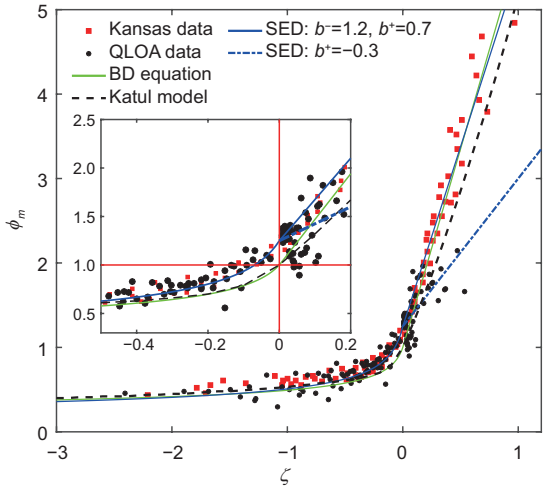

Figure 2 (Color online) Comparison of predicted ϕ_m by several theories with data. The inset is an amplification near $\zeta = 0$ and shows closer agreement of the SED prediction: eq. (31).

Finally, we validate our theory by directly comparing it with the measured mean speed profile containing QLOA data (we do not have Kansas mean speed profile data), see Figure 3, where the dashed lines correspond to predictions under the assumption $T_p = 0$, while the solid lines correspond to the model $T_p \approx -0.2S + 1.2B$ (for UC, $L < 0$) and $T_p \approx -0.2S - 0.3B$ (for SC, $L > 0$). Generally speaking, the solid lines agree better with the observed data for moderate z and large L (moderate heat flux). However, the fixed b model does not fit large z and small L (strong heat flux) data, satisfactorily. This indicates that b may be a varying parameter for nonequilibrium ASL from profile to profile. These small but clear deviations are not random, but reveal the fact that inactive parts of T_p may be varying with heat flux, which is reasonable. Indeed, our preliminary study shows that we can choose an optimal b for a much better fitting of all individual mean speed profiles (not shown here), which reflects the truly unsteady nature of open ASL physics. If the current model is further validated by more data, this work would open an avenue to interpret subtle deviations of the mean speed profiles from the log law and establish a framework to quantify the pressure transport in open ASL.

The magnitude of bB quantifies the top-down energy flux. The average T_p is estimated to be around 0.0017 m^2/s^3 when inserting dimensional quantities, which is consistent, in the order of magnitude with 1-3 $\times 10^{-3}$ obtained by energy spectrum filtering of low wavenumber parts interpreted as top-down effect [19]. It will be intriguing to verify these preliminary findings against more data.

5 Conclusion

In this work, we outline a new approach to the ASL analysis

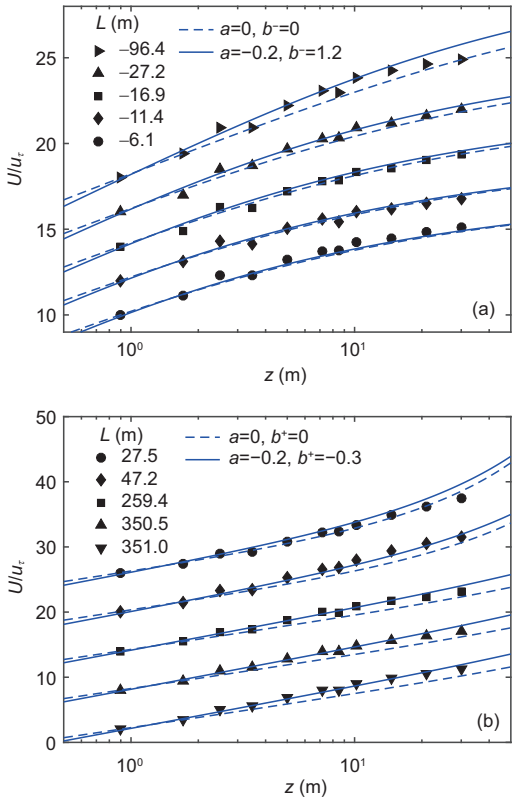

Figure 3 (Color online) Mean wind speed measurements at QLOA are compared with predictions of the present SED theory. (a) UC; (b) SC. Dashed lines correspond to the situation $T_p = 0$ and solid lines to the model: eq. (33), where $a = -0.2$, $b^- = 1.2$ for UC and $b^+ = -0.3$ for SC. For clarity of presentation, profiles are lifted upward by a fixed amount, to separate the profiles of different L.

based on a wall-induced dilation symmetry consideration of governing mean momentum and energy equation. This study shows that the SED theory has established a unified description of both UC and SC (including pressure transport). The preliminary success validates the concept of structural ensembles as subregions where the energy balance holds a specific mechanism and the stress length selects a specific power-law exponent in z. The concept is recently applied to describe laminar-turbulent transition accurately [32], which yields a remarkably precise drag prediction for aeronautic wings [33]. It is owing to our focus on the universal mechanism of symmetry-breaking from shear-dominated regime to buoyancy-dominated regime that $\phi_m(\zeta)$ can be derived in a unified way, for both UC and SC, which might seem impossible at first sight since the two conditions operate differently.

In summary, for the first time, we have derived an analytical form of ϕ_m which, under idealized condition of isotropy, yields a formula with no adjustable parameter (i.e., eq. (19)). The departure (and possible scattering) of data is then interpreted as a nonequilibrium effect of ASL due to pressure transport, which is considered to be constantly present in open ASL compared with canonical (wind tunnel) TBL. This interpretation is based on a model of pressure transport ($aS + bB$) with a pair of parameters (i.e., a and b), which are left to be determined by data. Limited testing against Kansas and QLOA data tends to favor the conclusion that in ASL, pressure transport is not small ($a = -0.2$). This consequently leads to a substantial correction of the Karman constant (from 0.45 to 0.36). Moreover, it concludes that the real ASL (even for $-z/L \ll 1$) is fundamentally different from the laboratory wind tunnel TBL due to its intrinsic openness with unavoidable pressure fluctuations. This assertion is somewhat striking since it is against the notion that ASL must go back to canonical TBL at a small heat flux. We believe that the present proposal deserves to be tested against more ASL data.

The achieved unified description via ℓ_{13} is more physical than ϕ_m since ℓ_{13} represents the size of dominant eddies contributing to momentum and energy transport, and hence is subject to wall-induced dilation symmetry constraint. Therefore, ℓ_{13} is a better variable than ϕ_m in capturing the system's underlying similarity structure. Once receiving further validation, it would represent a significant step for studying the nonequilibrium effect of ASL in a quantitative way.

This work was supported by the National Natural Science Foundation of China (Grant No. 91952201). The authors thank XiaoJing Zheng, and Guo-Hua Wang for sharing the QLOA data with us and for many helpful discussions.

1 I. Marusic, B. J. McKeon, P. A. Monkewitz, H. M. Nagib, A. J. Smits, and K. R. Sreenivasan, Phys. Fluids **22**, 065103 (2010).
2 J. C. Wyngaard, Annu. Rev. Fluid Mech. **24**, 205 (1992).
3 A. S. Monin, and A. M. Obukhov, Dok. Akad. Nauk. Sssr. **151**, 1963 (1954).
4 A. S. Monin, Annu. Rev. Fluid Mech. **2**, 225 (1970).
5 X. Li, N. Zimmerman, and M. Princevac, Bound.-Layer Meteorol. **129**, 115 (2008).
6 J. A. Businger, J. C. Wyngaard, Y. Izumi, and E. F. Bradley, J. Atmos. Sci. **28**, 181 (1971).
7 A. J. Dyer, Bound.-Layer Meteorol. **7**, 363 (1974).
8 D. M. Carl, T. C. Tarbell, and H. A. Panofsky, J. Atmos. Sci. **30**, 788 (1973).
9 H. A. Panofsky, Q. J. R. Meteorol. Soc. **87**, 109 (1961).
10 G. G. Katul, A. G. Konings, and A. Porporato, Phys. Rev. Lett. **107**, 268502 (2011).
11 G. Gioia, N. Guttenberg, N. Goldenfeld, and P. Chakraborty, Phys. Rev. Lett. **105**, 184501 (2010).
12 S. T. Salesky, G. G. Katul, and M. Chamecki, Phys. Fluids **25**, 105101 (2013).
13 D. Li, S. T. Salesky, and T. Banerjee, J. Fluid Mech. **797**, R3 (2016).
14 T. Banerjee, G. G. Katul, S. T. Salesky, and M. Chamecki, Q. J. R. Meteorol. Soc. **141**, 1699 (2015).
15 Z. S. She, X. Chen, Y. Wu, and F. Hussain, Acta Mech. Sin. **26**, 847 (2010).
16 Z. S. She, X. Chen, and F. Hussain, J. Fluid Mech. **827**, 322 (2017).
17 X. Chen, F. Hussain, and Z. S. She, J. Fluid Mech. **850**, 401 (2018).
18 X. Chen, and Z. S. She, Sci. China-Phys. Mech. Astron. **59**, 114711 (2016), arXiv: 1604.08257.
19 G. H. Wang, and X. J. Zheng, J. Fluid Mech. **802**, 464 (2016).

20 G. H. Wang, X. J. Zheng, and J. J. Tao, Phys. Fluids **29**, 061701 (2017).
21 H. Y. Liu, G. H. Wang, and X. J. Zheng, J. Fluid Mech. **861**, 585 (2019).
22 B. A. Kader, and A. M. Yaglom, J. Fluid Mech. **212**, 637 (1990).
23 J. C. R. Hunt, and J. F. Morrison, Eur. J. Mech.-B/Fluids **19**, 673 (2000).
24 U. Högström, J. C. R. Hunt, and A. S. Smedman, Bound.-Layer Meteorol. **103**, 101 (2002).
25 E. Bou-Zeid, X. Gao, C. Ansorge, and G. G. Katul, J. Fluid Mech. **856**, 61 (2018).
26 U. Högström, Bound.-Layer Meteorol. **78**, 215 (1996).
27 D. Li, and E. Bou-Zeid, Bound.-Layer Meteorol. **140**, 243 (2011).
28 C. Tong, and M. Ding, J. Atmos. Sci. **75**, 3691 (2018).
29 M. Chamecki, N. L. Dias, and L. S. Freire, Geophys. Res. Lett. **45**, 6734 (2018).
30 A. A. Townsend, J. Fluid Mech. **11**, 97 (1961).
31 U. Högström, Bound.-Layer Meteorol. **42**, 55 (1988).
32 M. J. Xiao, and Z. S. She, Sci. China-Phys. Mech. Astron. **62**, 994711 (2019).
33 M. J. Xiao, and Z. S. She, Acta Mech. Sin. **36**, 35 (2020).

Appendix Derivation of eqs. (13) and (14)

A1 Derivation of eq. (13)

According to ref. [16], the transition from one regime to another obeys a generalized ansatz:

$$\mathrm{I}_2 = \gamma_\mathrm{I}\mathrm{I}_1 + c(\mathrm{I}_1)^n, \tag{a1}$$

where I_1 and I_2 are (local) dilation invariants of the length function and its derivative, which are no longer constants (via a symmetry-breaking), when a transition takes place from one scaling regime to another. However, eq. (a1) holds. γ_I is the scaling exponent of the first regime before the transition. Here, two parameters, c and n, specify the transition location and sharpness.

Considering UC with a transition from the shear-dominated regime, $\gamma_\mathrm{I} = 1$, to the upward heat flux regime, we have $\mathrm{I}_1 = -\ell^\wedge_{13}/(-\zeta)^{4/3}$ and $\mathrm{I}_2 = -\dot{\ell}^\wedge_{13}/(-\zeta)^{1/3}$. Substituting the last two expressions into eq. (a1), we obtain

$$\frac{-\dot{\ell}^\wedge_{13}}{(-\zeta)^{1/3}} = \frac{-\ell^\wedge_{13}}{(-\zeta)^{4/3}} + c\left(\frac{-\ell^\wedge_{13}}{(-\zeta)^{4/3}}\right)^n, \tag{a2}$$

where $\dot{\ell}^\wedge_{13} = \mathrm{d}\ell^\wedge_{13}/\mathrm{d}(-\zeta)$. Introduce a new variable $y = \ell^\wedge_{13}/\zeta$, so that $\ell^\wedge_{13} = y\zeta$, $\dot{\ell}^\wedge_{13} = \dot{y}\zeta - y$, then eq. (a2) is simplified to

$$\frac{\dot{y}}{y^n} = c(-\zeta)^{\frac{-2-n}{3}}. \tag{a3}$$

If $n \neq 1$ and $\dot{y} = \mathrm{d}y/\mathrm{d}(-\zeta)$, an integration then yields

$$\frac{1}{1-n}y^{1-n} = A_0 + c\frac{3}{1-n}(-\zeta)^{\frac{1-n}{3}}. \tag{a4}$$

Substitute back $\ell^\wedge_{13}$, we have

$$\ell^\wedge_{13} = [A_0(1-n)]^{\frac{1}{1-n}}\,\zeta\left(1 + \frac{3c}{A_0(1-n)}(-\zeta)^{\frac{1-n}{3}}\right)^{\frac{1}{1-n}}. \tag{a5}$$

Note that the exponent $(1-n)/3$ denotes sharpness of the transition. Let it be 1 (which is the only free parameter) and denote the up-front coefficient by κ, i.e.,

$$\frac{1-n}{3} = 1, \qquad [A_0(1-n)]^{\frac{1}{1-n}} = \kappa,$$

or $n = -2$ and $A_0 = \kappa^3/3$. We further define $\zeta_\mathrm{UC} = \kappa^3/3c$. The final expression of $\ell^\wedge_{13}$ is then

$$\ell^\wedge_{13} = \kappa\zeta\left(1 + \frac{-\zeta}{\zeta_\mathrm{UC}}\right)^{1/3}. \tag{a6}$$

A2 Derivation of eq. (14)

The transition from shear-dominated regime, $\gamma_I = 1$, to the downward heat flux regime can be derived similarly as in Appendix A1. Here, we have $\mathrm{I}_1 = \ell^\wedge_{13}$ and $\mathrm{I}_2 = (\mathrm{d}\ell^\wedge_{13}/\mathrm{d}\zeta)/\zeta^{-1}$. Substituting the last two expressions into eq. (a1), it can be verified that

$$\ell^\wedge_{13} = \kappa\zeta\left(1 + \frac{\zeta}{\zeta_\mathrm{SC}}\right)^{-1}, \tag{a7}$$

where we set $c = -1/\kappa\zeta_\mathrm{SC}$ and $n = 2$.